Multi-Band Planar Antennas: A Comparative Study

Aleš ČÁP, Zbyněk RAIDA, Eduardo de las HERAS PALMERO, Roberto LAMADRID RUIZ

Dept. of Radio Electronics, Brno University of Technology, Purkyňova 118, 612 00 Brno, Czech Republic

acap@seznam.cz, raida@feec.vutbr.cz, roberto_lamadrid@hotmail.com, eherasp@hotmail.com

Abstract. *In the paper, four different planar multi-band antennas are designed, modeled, fabricated, and measured. Parameters of the antennas are in detail compared to demonstrate advantages and disadvantages of different solutions. Discussions are supported by results of the modal and full-wave analyses of antennas.*

The classical patch antenna is a basic building block of compared antennas. The multi-band behavior is achieved by etching perturbation slots to the patch, which influence resonant current distributions.

The antennas are designed for GSM bands (900 MHz, 1 800 MHz), and for the Bluetooth band (2 400 MHz).

Keywords

Multi-band planar antennas, perturbation slots, modal analysis, full-wave analysis, GSM, Bluetooth.

1. Introduction

Today's radio communication is dominantly of the broad- and multi-band nature. Antenna designers are therefore enforced to design antennas matched to the operation in multi-bands. Considering mobile communication, the designed antennas have to be compact. And that is why the planar technology is so popular.

In the open literature, an extreme care is devoted to the design of planar multi-band antennas: several monographs have been published [1]–[3]; plenty of papers have been appearing in journals and conference proceedings. In our contribution, we concentrate on antennas, which achieve the multi-band operation by etching perturbation slots to the rectangular patch. Other techniques of constructing multi-band antennas (fractal approaches, planar radiators in different distances from the ground plane, etc.) are out of the scope of this paper.

Due to the quite high number of papers devoted to proposing novel, advantageous layouts of patch multi-band antennas, a detailed overview can be hardly done, and any layout can be hardly proven as the original one. For illustration, we overview the development published in the

IEEE Transactions on Antennas and Propagation in 2005, and we are subjectively commenting them:

- In [4], an antenna composed of inverted F and L strip lines was designed to operate in WLAN frequency bands f_1 = 2.45 GHz (G_1 = 0.9 dBi, and B_1 = 4.1 % for VSWR = 2) and f_2 = 5.2 GHz (G_2 = 1.7 dBi, and B_2 = 31.8 % for VSWR = 2). Current distributions were not provided; attention was turned to tuning the antenna by changing dimensions of strips.

- In [5], a classical Planar Inverted-F (PIF) antenna was modified by etching plunged in parallel U-slots of decreasing size, and by inserting a capacitive plate between the radiating element and the ground plane. Using 4 U-slots, resonances in 4 operation bands were achieved (GSM and WLAN). The bandwidths varied from 3 % to 9 %, gains and current distributions were not provided. The antenna was tuned by changing positions and sizes of U-slots and the capacitive plate.

- In [6], a standard PIF antenna was used to cover GSM frequency bands, and was combined with an Inverted F (IF) antenna for the operation in the GPS band. The novelty consisted in optimizing the co-existence of both the antennas.

- In [7], L-slot, dual L-slot, and inverted T-slot antennas were experimentally investigated. Changing dimensions of slots, antennas were tuned for operating in two frequency bands with the emphasis to the maximum width of the frequency band (up to 80 % for the return loss −10 dB). Gains and current distributions were not provided.

- In [8], a triangular patch with two slots parallel with edges was proposed. The antenna was excited in the patch center by the coaxial probe. The antenna was designed for WLAN frequency bands. Attention was turned to measuring directivity patterns.

We can conclude that the discussed multi-band antennas differed in various perturbation slots and elements, which were etched to the patch as the basic antenna element. The proposed antenna layouts were compared to the conventional patch antenna to demonstrate their advantages and drawbacks.

Papers were usually conceived purely practically: a basic shape of perturbation slots was empirically proposed, the antenna was modeled and tuned, and in the limited cases, modeling results were experimentally verified.

In this paper, we concentrate on mutual comparison of four multi-band antennas (Fig.1). The L-slot antenna plays the role of the dual-band reference antenna. The double-extended antenna can be understood as a capacitive extension of the patch. In case of the U-slot antenna, the patch is broken by the slot to a smaller resonator (higher frequencies) and to a larger one (lowers frequencies). Finally, the double-U antenna is based on similar principles as described in [5], but the slots are oriented opposite each other.

Fig. 1. The photograph of compared antennas: the L-slot antenna (top left), the double-extended antenna (bottom left), the U-slot antenna (top right), and the double-U antenna (bottom right).

Comparing antennas, effects of different perturbation elements to the impedance matching, radiation and polarization properties of antennas can be observed.

In Section 2, the compared antennas are in detail described. Section 3 brings results of the modal analysis of investigated antennas. Section 4 presents results of full-wave analysis and compares them with results of modal analysis. Computed current distributions and polarization effects are discussed, computed frequency responses of reflection coefficient and directivity patterns are confronted with results of measurements. Section 5 concludes the paper.
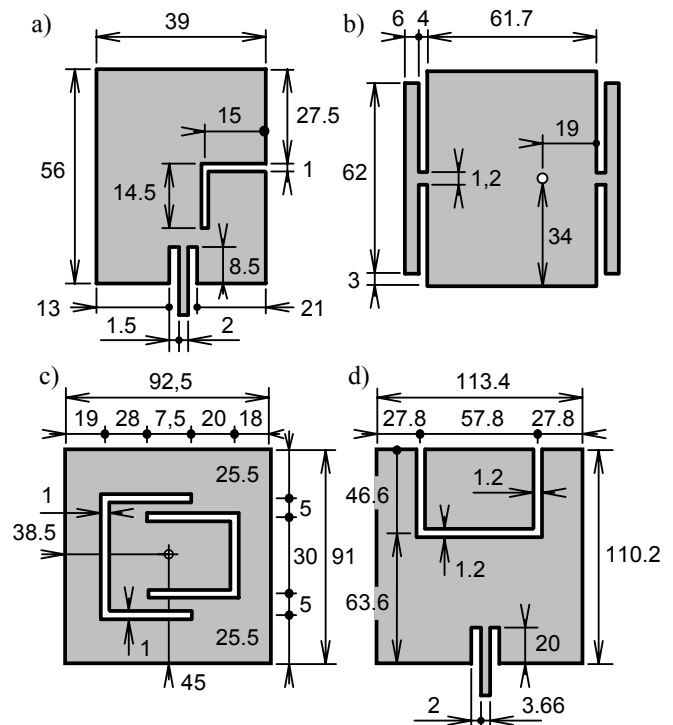
2. Antenna Design

In the comparative study, four planar antennas are considered (see Fig. 1).

The L-slot antenna is fed by the microstrip line. Antenna dimensions are depicted in Fig. 2a. The antenna is designed for the substrate FR4 (dielectric constant is $\varepsilon_r = 4.17$, substrate height $h = 3.08$ mm). Required operation bands are around central frequencies $f_2 = 1\,830$ MHz and $f_3 = 2\,430$ MHz.

The double-extended antenna is fed by the coaxial probe. Antenna dimensions are depicted in Fig. 2b. The antenna is designed for the substrate CuClad 217 (dielectric constant $\varepsilon_r = 2.17$, substrate height $h = 4.62$ mm). Required operation bands are around central frequencies $f_1 = 924$ MHz and $f_2 = 1\,786$ MHz.

The double-U antenna is fed by the coaxial probe. Antenna dimensions are depicted in Fig. 2c. The antenna is designed for the substrate CuClad 217 (dielectric constant $\varepsilon_r = 2.17$, substrate height $h = 1.54$ mm). Required operation bands are around central frequencies $f_1 = 932$ MHz and $f_2 = 1\,795$ MHz.

The U-slot antenna is fed by the microstrip line. Antenna dimensions are depicted in Fig. 2d. The antenna is designed for the substrate CuClad 217 (dielectric constant $\varepsilon_r = 2.17$, substrate height $h = 1.54$ mm). Required operation bands are around central frequencies $f_1 = 885$ MHz, $f_2 = 1\,875$ MHz, and $f_3 = 2\,460$ MHz.

Fig. 2. Dimensions (in millimeters) of the layout of the investigated antennas: a) the L-slot antenna, b) the double-extended antenna, c) the double-U antenna, d) the U-slot antenna. Dimensions are measured from the center of slots (except of slot widths).

For the described antennas, the modal analysis is performed in FEMLAB (see Section 3). Then, the antennas are modeled in CST Microwave Studio and Zeland IE3D, are fabricated and measured (see Section 4).

3. Modal Analysis

In order to investigate resonances of the antennas of interest, the modal analysis is performed. The antenna is modeled like a longitudinally homogeneous dielectric waveguide which cross section is identical with the shape of the antenna element. Permittivity of the waveguide equals to the permittivity of the antenna substrate. Side walls of the waveguide are assumed to be perfectly magnetically conductive.

In the waveguide, the propagation of the transversally magnetic modes is assumed. The analysis is based on computing the distribution of the longitudinal component of the electric field intensity, which is perpendicular both to the ground plane and to the planar antenna element. The analysis is performed in FEMLAB 3.1.

The described model corresponds to the well-known cavity model of planar antennas.

patch		L-slot
mode	f [GHz]	f [GHz]
TM01	1.311	0.887
TM10	1.882	1.603
TM11	2.294	2.038
TM02	2.622	2.630

Tab. 1. Comparison of resonance frequencies of the patch without the L-slot and the patch completed by the L-slot.

In Table 1, modes and resonant frequencies of the patch 39 × 56 mm without slots are given in the left-hand column. In the right-hand column, resonant frequencies of the L-slot antenna are given. Here, modes are not determined because the relatively complicated field distribution makes the mode identification rather difficult.
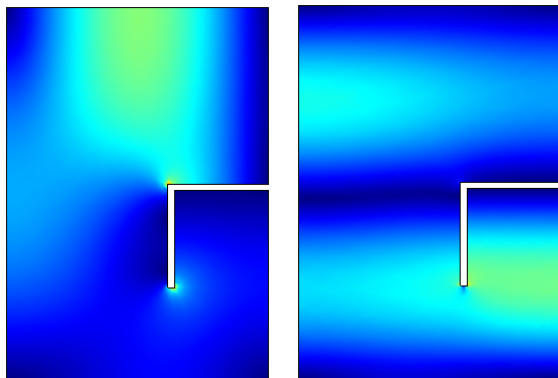

Fig. 3. Operation modes of the L-slot antenna. Distribution of the magnitude of the current density on the antenna element on f_2 = 2.038 GHz (left) and f_3 = 2.630 GHz (right).

The L-slot antenna is designed for the operation in frequency bands f_2 = 1 830 MHz and f_3 = 2 430 MHz. Etching the L-slot to the patch and changing dimensions of the slot, the antenna is tuned to resonate on frequencies 2 038 MHz and 2 630 MHz, which correspond satisfactorily to the required operation frequencies (deviations about 10 %).

The modal analysis ignores the way of exciting the antenna (the feeding microstrip, and the matching slots on the sides of the feeding microstrip are not included). Moreover, the electromagnetic field outside the substrate is not considered (the field in dielectrics is isolated by perfect magnetic walls from the surroundings). Therefore the error in resonant frequencies reaches up to 10 %.

On the other hand, the modal analysis can reveal modes, which are hidden in the full-wave model (due to the position of the excitation, potential modes are not excited).

The distribution of the current density on the antenna element is depicted in Fig. 3. On the lower operation frequency, the current is concentrated in the upper part of the patch (the lower part is *shielded* by the L-slot). On the higher frequency, the current distribution corresponds to the TM02 mode of the patch.

Modes and resonant frequencies of the patch 61.7 × 68.0 mm without extensions are given in Table 2 (left-hand column). In the right-hand column, resonant frequencies of the patch with extensions can be found. Obviously, differences between both the antennas are negligible in resonant frequencies, and also in current distributions (see Fig.4).

patch		extended
mode	f [GHz]	f [GHz]
		0.737
TM01	1.496	1.497
TM10	1.649	1.642
TM11	2.227	1.705

Tab. 2. Comparison of resonance frequencies of the patch without extensions and the double-extended patch.

The double-extended antenna is designed for operating in frequency bands f_1 = 924 MHz and f_2 = 1 786 MHz (modes TM10 and TM30). Resonant frequencies obtained from the modal analysis differ for up to 25 %.
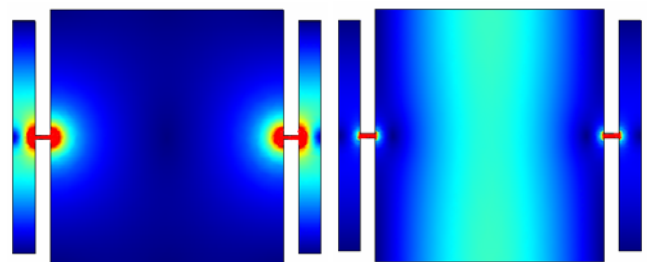

Fig. 4. Operation modes of the double extended patch. Distribution of the magnitude of the current density on the antenna element on f_1 = 0.737 GHz (left) and f_2 = 1.705 GHz (right).

The modal analysis shows that the first mode of the extended antenna appears below the critical frequency of the dominant mode of the patch without extensions. The upper mode of the extended antenna is close to the mode TM10 of the patch.

patch		double-U
mode	f [GHz]	f [GHz]
		0.549
		0.776
TM10	1.100	**0.887**
TM01	1.118	1.415
TM11	1.569	1.784
TM20	2.200	**1.851**

Tab. 3. Comparison of resonance frequencies of the patch without slots and the double-U antenna.

In Table 3, we compare resonant frequencies of the patch 92.5×91.0 mm without slots and the double-U antenna. For the operation, the mode TM10 is chosen: the whole patch resonates on frequency $f_1 = 887$ MHz, and the area inside U-slots resonates on $f_2 = 1\,851$ MHz (Fig. 5). Changing dimensions of U-slots, the antenna can be tuned. Adding U-slots, operation can be extended to further bands.
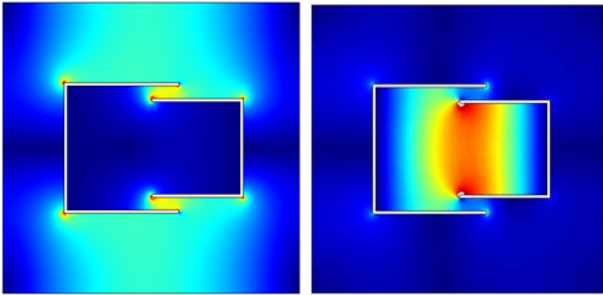

Fig. 5. Operation modes of the double-U antenna. Distribution of the magnitude of the current density on the antenna element on $f_1 = 0.887$ GHz (left) and $f_2 = 1.851$ GHz (right).

Resonant frequencies of the double-U antenna differ from the desired ones $f_1 = 932$ MHz and $f_2 = 1\,795$ MHz for less than 5 %.

patch		U-slot
mode	f [GHz]	f [GHz]
TM10	0.897	0.606
TM01	0.923	**0.884**
TM11	1.288	1.160
TM20	1.795	1.702
TM02	1.847	1.791
TM21	2.018	**1.867**
TM12	2.053	1.960
TM22	2.575	2.231
TM30	2.692	**2.376**

Tab. 4. Comparison of resonance frequencies of the patch without slots and the U-slot antenna.

Resonant frequencies of the patch 113.4×110.2 mm without slots and the U-slot antenna are compared in Table 4. The desired frequencies $f_1 = 885$ MHz, $f_2 = 1.875$ GHz, and $f_3 = 2.46$ GHz differ from resonant ones for less than 4 %. Observing current distributions (Fig. 6), resonant modes can be hardly classified.
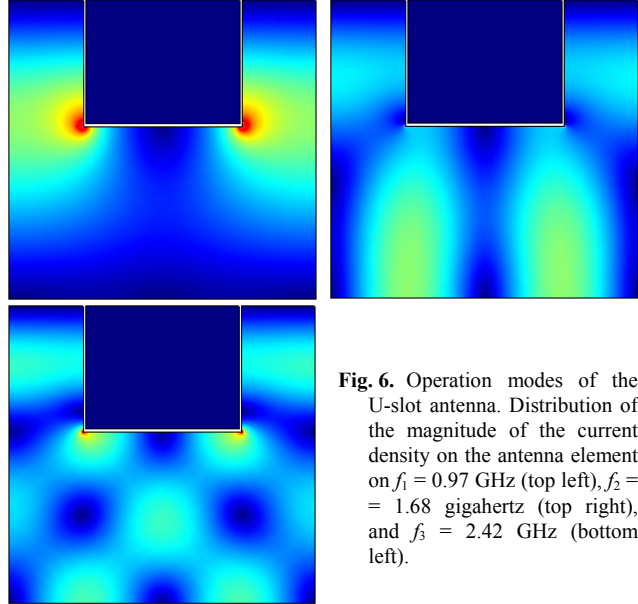

Fig. 6. Operation modes of the U-slot antenna. Distribution of the magnitude of the current density on the antenna element on $f_1 = 0.97$ GHz (top left), $f_2 = 1.68$ gigahertz (top right), and $f_3 = 2.42$ GHz (bottom left).

In the next chapter, results of the modal analysis are verified by the full-wave analysis in CST Microwave Studio and Zeland IE3D[1].

4.   Full-Wave Analysis

Since Zeland IE3D is based on the moment method, and the current distribution on antenna elements is the primary quantity computed, we use this program to analyze current distributions (Figures 7 to 11). The distributions computed are compared with results of the modal analysis.

---

[1]   In FEMLAB, the scalar wave equation for the longitudinal component of the electric field intensity is solved using frequency domain finite elements. The propagation constant is assumed being zero to obtain critical frequencies.

In CST Microwave Studio, time-domain Maxwell's equations are solved using time-domain finite differences. As a result, electromagnetic field in antenna surroundings is obtained, and current distributions can be consequently computed.

In Zeland IE3D, Maxwell's equations in the integral form are solved using the frequency-domain moment method. The current distribution on the antenna elements is obtained as a result of the analysis, and antenna parameters are evaluated secondarily.
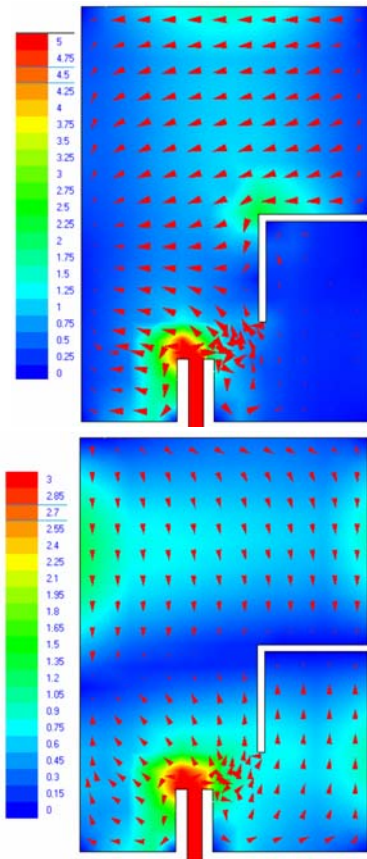
Fig. 7. Current distribution on the L-slot antenna: $f_2 = 1\ 830$ MHz (top), $f_3 = 2\ 430$ MHz (bottom).
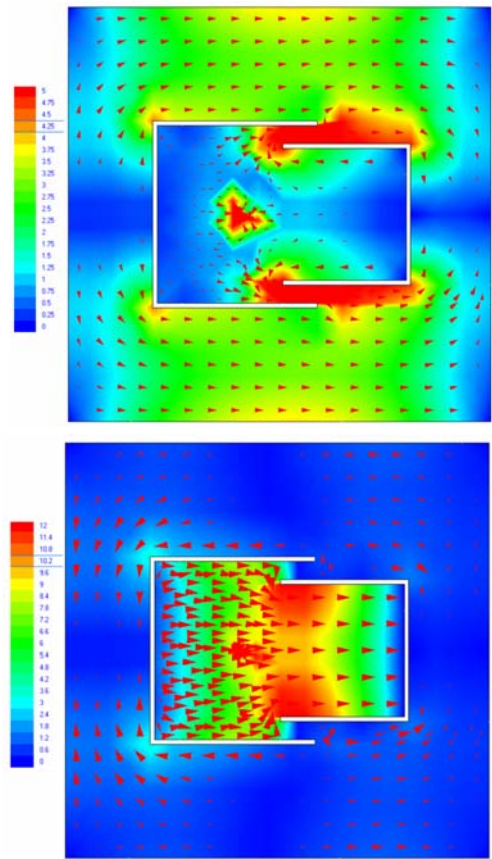

Fig. 9. Current distribution on the double-U antenna: $f_1 = 932$ MHz (top), $f_2 = 1\ 795$ MHz (bottom).
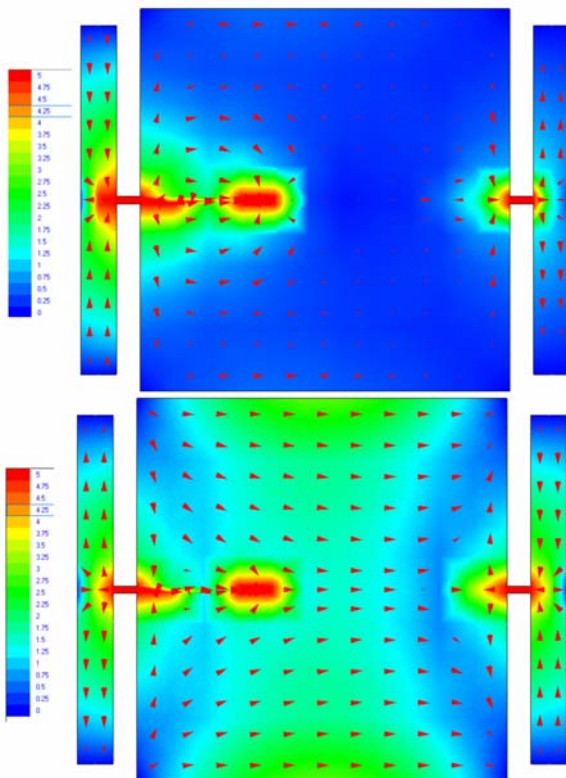

Fig. 8. Current distribution on the double-extended antenna: $f_1 = 924$ MHz (top), $f_2 = 1\ 786$ MHz (bottom).
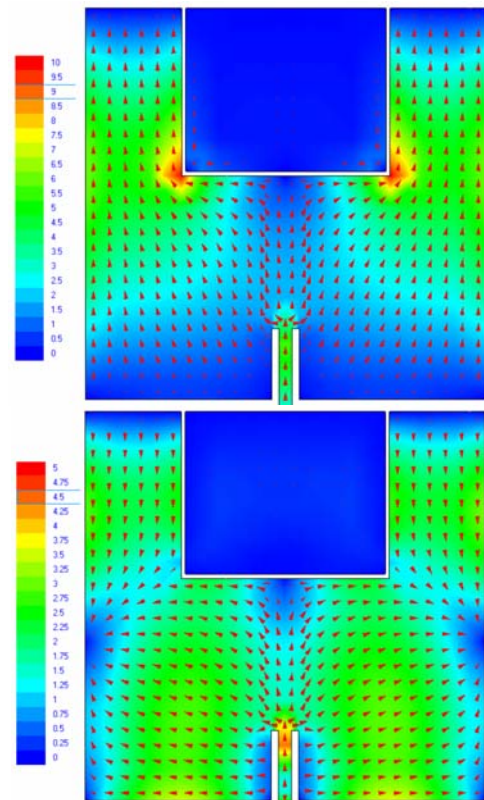

Fig. 10. Current distribution on the U-slot antenna: $f_1 = 885$ MHz (top), $f_2 = 1\ 875$ MHz (bottom).
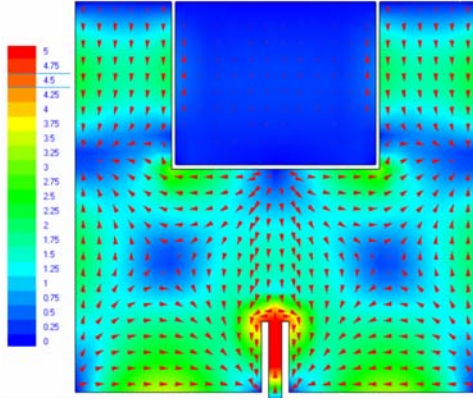
Fig. 11. Current distribution on the U-slot antenna: f_3 = 2 460 MHz.

The current distributions are discussed from the viewpoint of the polarization properties of antennas. Discussions are validated computing the maximum value of the cross-polarization in CST Microwave Studio, which computes the electromagnetic field in the surrounding of the antenna as the primary quantity.

Frequency responses of the reflection coefficient of the designed antennas are evaluated to verify their proper tuning for the required operation bands (Figures 12 to 15). Reflection coefficients are computed by CST Microwave Studio.

We also visualize three-dimensional (3D) directivity patterns (CST Microwave Studio) and compare them with measurements (Figures 16 to 20).

4.1 Current Distributions

The current density of the investigated L-slot antenna (Fig. 7) contains dominantly x-components in the frequency band f_2 (the mode appearing can be considered TM10 in the area above the horizontal part of the L-slot), and dominantly y-components in the frequency band f_3 (the mode TM02 slightly perturbed by the vertical part of the slot). Considering the communication in the vertical polarization, the L-slot antenna exhibits the cross-polarization up to 1.9 dBi in the lower band, and up to −15.9 dBi in the upper band. The different polarizations in the investigated frequency bands are disadvantage of the presented design.

Computing the magnitude of currents, a quite good correspondence between the full-wave analysis (Fig. 7) and the modal one (Fig. 3) can be observed: the longest current vectors appear above the L-slot in the band f_2, and the current distribution corresponds to the mode TM02 in the band f_3.

Observing current distributions of the double-extended antenna (Fig. 8), the strongest currents are concentrated on the edges of the side slots (y-components) and in the neck connecting the patch and rectangular side elements (x-components). The y-components mutually compensate their radiation due to the opposite current orientation on the opposite edges of slots.

The side elements can be understood as the capacitive prolongation of the patch, which increases the dominant x-component of the current on the patch. Hence, the x-polarization is dominant in both the frequency bands. Considering the communication in the horizontal polarization, the antenna exhibits the cross-polarization up to −16.1 dBi the in lower band, and the cross-polarization up to −15.4 dBi in the upper band.

The modal analysis (Fig. 4) reveals the modes TM10 and TM30 on the antenna element, which corresponds quite well to current distributions depicted in Fig. 8.

In case of the double-U antenna (Fig. 9), the whole patch resonates on the lower frequency f_1, and the currents are concentrated in the area out of the U-slots. On the upper frequency f_2, currents in the area inside the U-slots play the dominant role. In both bands, x-polarization dominates. Considering the communication in the horizontal polarization, the antenna exhibits the cross-polarization up to −16.9 dBi the in lower band, and the cross-polarization up to −9.0 dBi in the upper band.

The modal analysis (Fig. 5) shows similar results: there are negligible currents inside the U-slots in the lower band, and outside the U-slots in the higher band.

Finally, the current distribution of the U-slot antenna (Figures 10, 11) shows us that the upper segment of the antenna does not radiate in any frequency band. Thanks to this segment, the antenna can be well tuned for multi-band operation.

In the lowest band f_1, the mode TM01 appears on the antenna element with the minimal value of the x-component (the cross-polarization is lower than −16.2 dBi).

Approaching frequency bands f_2 and f_3, higher modes of the current distribution are excited, and y-components of currents are increasing. The polarization purity is therefore degraded in the higher bands (cross-polarization reaches up to −2 dBi on f_2 and up to −3.6 dBi on f_3).

From the viewpoint of the polarization purity in all the frequency bands, the double-U antenna seems to provide the best results. The U-slot antenna excels in covering three frequency bands.

4.2 Reflection Coefficients

In the first experiment, reflection coefficient at the antenna input was measured and compared with the results of the full-wave analysis.

In case of the L-slot antenna (Fig. 12), CST revealed deep minims of s_{11} (−15 dB) on frequencies 1 500 MHz and 2 446 MHz. Further minim (−11 dB) was revealed on 1 829 MHz, and a shallow minim (−4 dB) on 966 MHz. The L-slot antenna was designed for bands around frequencies f_2 = 1 830 MHz and f_3 = 2 430 MHz.
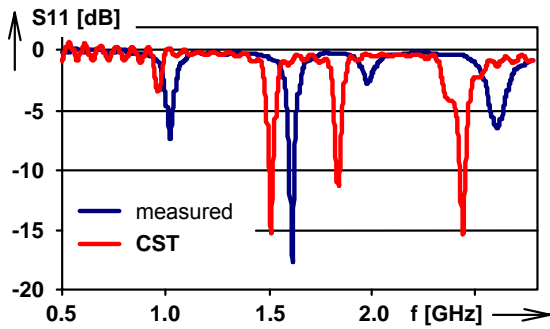
Fig. 12. Reflection coefficient at the input of the L-slot antenna.

The measured minims exhibit frequency shifts from 60 megahertz (the band 900 MHz) to 161 MHz (the band 2 400 MHz) compared to the numerical analysis. Moreover, the value of s_{11} is very high on the frequencies of interest $f_2 = 1\,830$ MHz and $f_3 = 2\,430$ MHz.

Measurements and modeling of the double-extended antenna (Fig. 13) showed a good agreement in resonance frequencies and differences in values of s_{11} on them: on 929 MHz (–16 dB measured versus –8 dB computed), on 1 189 MHz (–3 dB measured versus –19 dB computed), on 1 795 MHz (–9 dB measured versus –36 dB computed). The double extended antenna was designed for frequencies $f_1 = 924$ MHz, $f_2 = 1\,786$ MHz.
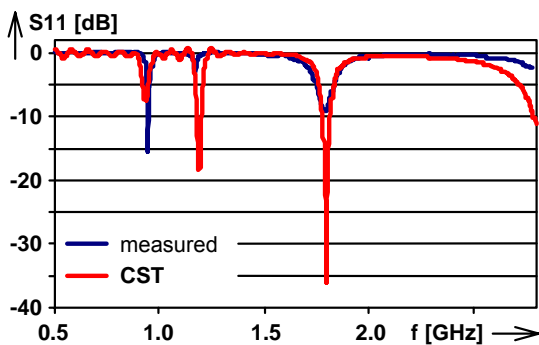
Fig. 13. Reflection coefficient at the input of the double-extended antenna.

Observing the s_{11} frequency response of the double-U antenna (Fig. 14), a good agreement of resonance frequencies obtained by simulation and measurement can be stated. On the lower resonant frequency, the value of s_{11} is relatively small (–10 dB in simulation, and –4dB in measurement). On the higher frequency, the situation is better (–27 dB in simulation, and –16 dB in measurement).
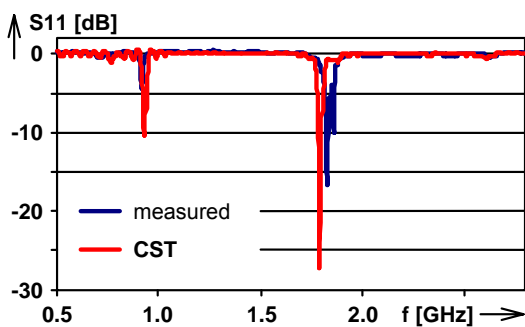
Fig. 14. Reflection coefficient at the input of the double-U antenna.

Finally, the agreement between the computation and the experiment is good for the U-slot antenna, and the value of s_{11} is smaller compared to the double-U antenna (see Fig.15). The U-slot antenna enables us to tune it for three frequency bands.
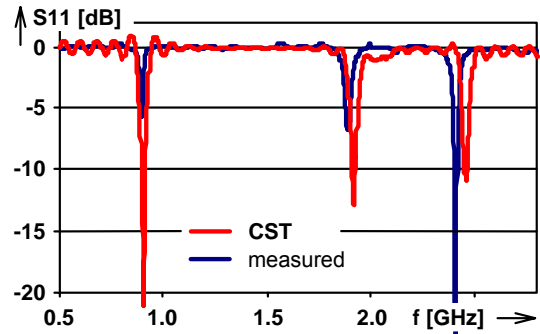
Fig. 15. Reflection coefficient at the input of the U-slot antenna.

4.3 Directivity Patterns

The second experiment was devoted to the verification of directivity patterns computations. The measurements were performed in the anechoic chamber of the Czech radar company ERA Pardubice.

In Figures 16 to 20, three-dimensional directivity patterns computed by CST Microwave Studio are depicted on the top, and measured patterns in the E plane and the H one are given below. In patterns, the magnitude of the gain is depicted.
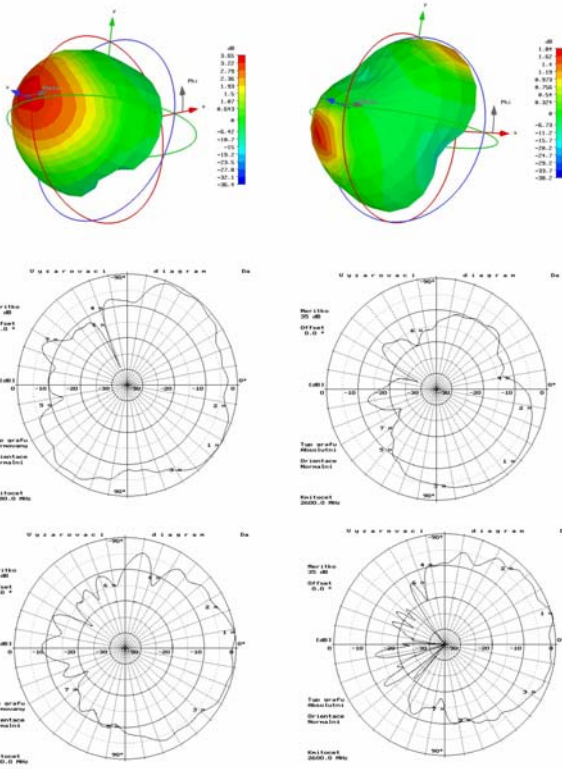
In 3D figures, the directivity patterns in E-plane are obtained when following the red circle, and patterns in H-plane can be seen when moving along the green circle. Following the circles in 3D patterns, the corresponding run of the gain can be observed in the measured two-dimensional patterns.

In most cases, the directivity pattern consists of a wide beam oriented perpendicularly to the antenna surface (the double-extended antenna in Fig. 17, the double-U antenna in Fig. 18, and the U-slot antenna in Fig. 19 on the frequency $f_1 = 890$ MHz). On the frequency $f_2 = 1\,913$ megahertz, the U-slot antenna exhibits a deep minim of the directivity pattern in the perpendicular direction, and on the frequency $f_3 = 2\,400$ MHz, the main lobe is turned for 35° in the E plane. The worst directivity properties are shown by the L-slot antenna (see Fig. 16).
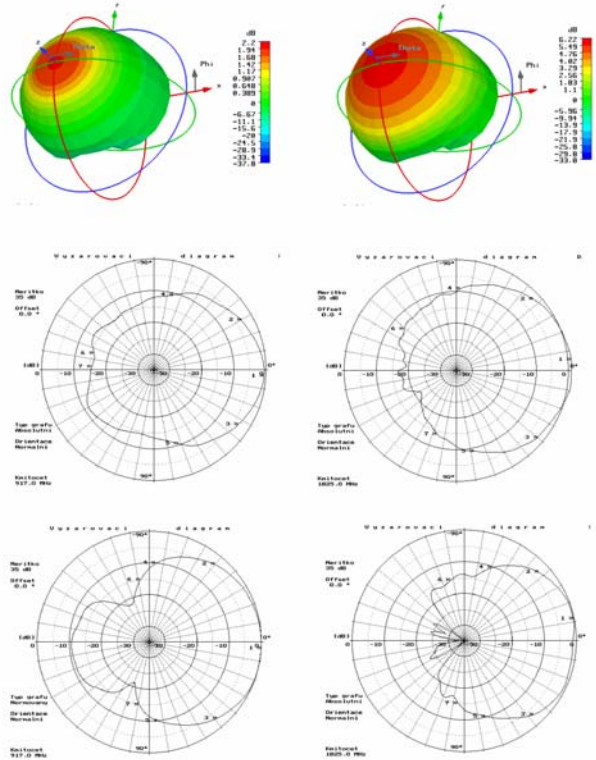
5. Conclusions

Comparing the investigated antennas, we can state the following conclusion:
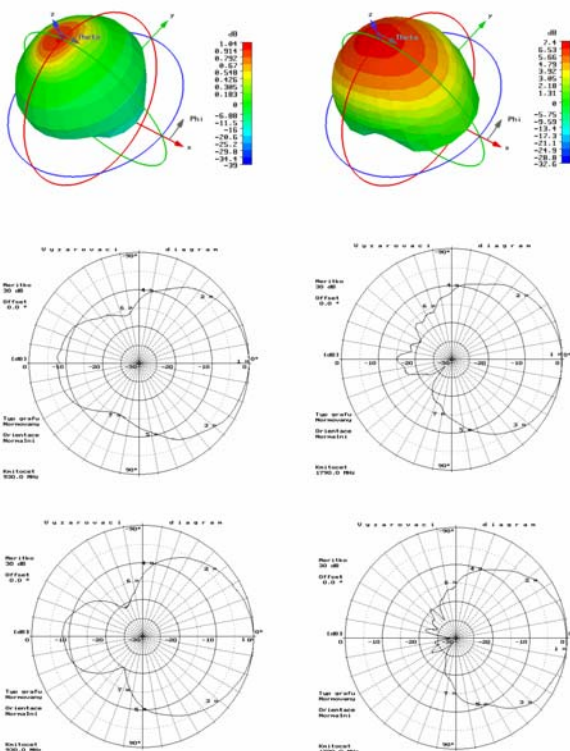
- The double-U antenna exhibits the best parameters (directivity patterns without deformations, sufficient polarization purity). On the other hand, only two frequency bands are covered.
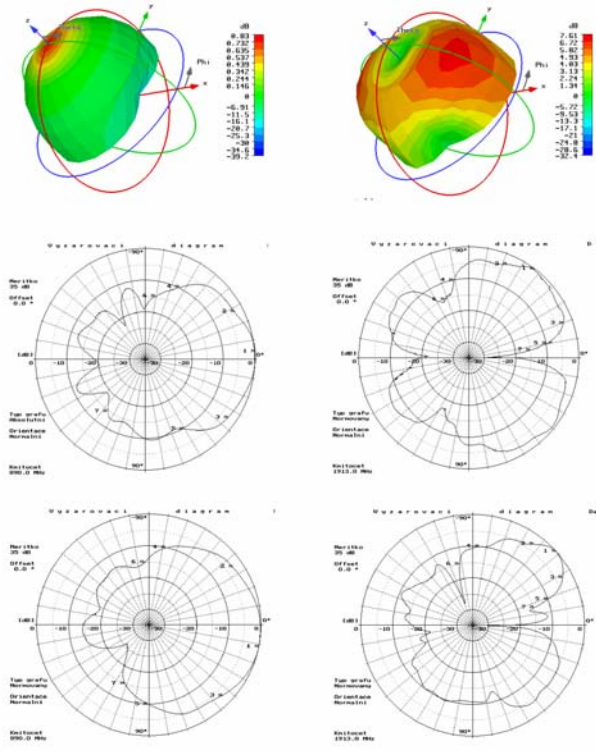
Fig. 16. Directivity patterns of the L-slot antenna on frequency $f_2 = 1\ 980$ MHz (left) and $f_3 = 2\ 600$ MHz (right): computed (top), measured in the E-plane (center), measured in the H-plane (bottom).

Fig. 18. Directivity patterns of the double-U-antenna on the frequency $f_1 = 917$ MHz (left) and $f_2 = 1\ 825$ MHz (right): computed (top), measured in the E-plane (center), measured in the H-plane (bottom).

Fig. 17. Directivity patterns of the double-extended antenna on the frequency $f_1 = 930$ MHz (left) and $f_2 = 1\ 790$ MHz (right): computed (top), measured in the E-plane (center), measured in the H-plane (bottom).

Fig. 19. Directivity patterns of the U-slot antenna on frequency $f_1 = 890$ MHz (left) and $f_2 = 1\ 913$ MHz (right): computed (top), measured in the E-plane (center), measured in the H-plane (bottom).
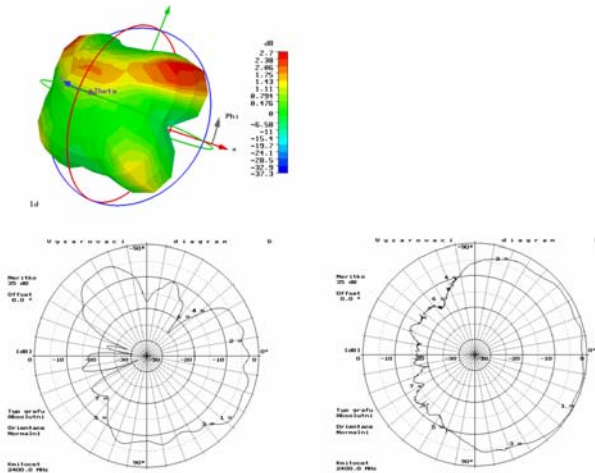
Fig. 20. Directivity patterns of the U-slot antenna on frequency $f = 2\,400$ MHz: computed (top), measured in the E-plane (bottom, left), measured in the H-plane (bottom, right).

The described properties of the double-U antenna are given by its construction. The antenna is composed of two patches: the larger one resonates on lower frequencies, and the smaller one on higher frequencies.

We can state the hypothesis here, that a three-band antenna can be composed of three patches (another couple of U-slots have to be added into the layout).

- The double-extended antenna provides also good parameters: directivity patterns are uncorrupted, and the polarization is sufficiently pure.

  Unfortunately, the primary principle of the antenna (capacitive extensions enhance currents on the patch) enables us to reach more than the two-band operation of the antenna by exciting higher current modes only. Moreover, efficiency of the antenna is very poor in the lower frequency band (see Tab .5).

- The U-slot antenna excels in covering three frequency bands. The antenna is well tuned by dimensions of the rectangular sub-element, which does not radiate itself.

  The multi-band operation is achieved by exciting higher modes of current distribution. This fact causes relatively low polarization purity, and the corruption of directivity patterns in higher frequency bands.

- The L-slot antenna provided the worst results. Even the match between the computer simulations and measurements was not good. We therefore exclude the L-slot antenna from further comparisons.

The numeric parameters of the investigated antennas are given in Table 5.

Considering measured numeric parameters, even here the double-U antenna provides the best results except of the value of reflection coefficient in the lower band: due to its measured value –4.41 dB, we are not able to determine the bandwidth given by the limit $s_{11} = -5$ dB.

	extended	double-U	U-slot
f_1 [MHz]	930	917	890
B_1 [MHz]	17.0	- - -	7.2
B_1 [%]	1.8	- - -	0.8
$s_{11,1}$ [dB]	−15.54	−4.41	−5.69
G_1 [dBi]	1.04	2.20	0.83
$e_{r,1}$ [%]	32.9	57.3	63.8
$e_{a,1}$ [%]	1.4	49.0	28.1
f_2 [MHz]	1 790	1 825	1 913
B_2 [MHz]	87.5	51.38	21.0
B_2 [%]	4.9	2.8	1.1
$s_{11,2}$ [dB]	−9.17	−16.68	−6.78
G_2 [dBi]	7.40	6.22	7.61
$e_{r,2}$ [%]	82.8	78.5	81.9
$e_{a,2}$ [%]	75.3	39.1	71.9
f_3 [MHz]	- - -	- - -	2 400
B_3 [MHz]	- - -	- - -	27.0
B_3 [%]	- - -	- - -	1.1
$s_{11,3}$ [dB]	- - -	- - -	−23.65
G_3 [dBi]	- - -	- - -	2.70
$e_{r,3}$ [%]	- - -	- - -	75.2
$e_{a,3}$ [%]	- - -	- - -	18.3

Tab. 5. The measured parameters of investigated antennas (the L-slot antenna excluded): the operation frequency of the m-the frequency band f_m, bandwidth of the m-th frequency band B_m (given by $s_{11} = -5$ dB), reflection coefficient on the m-th operation frequency $s_{11,m}$, and gain on the m-th operation frequency related to the isotropic radiator G_m. The computed parameters of investigated antennas (the L-slot antenna excluded): radiation efficiency on the m-th operation frequency $e_{r,m}$, and antenna efficiency on the m-th operation frequency $e_{a,m}$.

In order to reach the desired value of the reflection coefficient in the lower frequency band, advanced optimization techniques have to be exploited. In the formulation of the optimization task, the required reflection properties have to be included into the objective function (the penalization of $s_{11} > -5$ dB), or the optimization problem has to be completed by a linear inequality constraint $s_{11} < -5$ dB.

The measurements show an extremely narrow bandwidth of the designed multi-band antennas: the bandwidth varies from 0.8 % to 4.9 %. The results illustrate the fact that introducing perturbation elements to reach the multi-band behavior shortens the even short bandwidth of patch antennas [1].

Acknowledgements

References

[1] GARG, B., BAHL, I. *Microstrip Antenna Design Handbook*. Norwood: Artech House, 2001.

[2] KUMAR, G., RAY, K. P. *Broadband Microstrip Antennas*. Norwood: Artech House, 2003.

[3] WONG, K. L. *Compact and Broadband Microstrip Antennas*. New York: J. Wiley and Sons, 2002.

[4] NAKANO, H., SATO, Y., HIROAKI, M., YAMAUCHI, J. An inverted FL antenna for dual-frequency operation. *IEEE Transactions on Antennas and Propagation*. 2005, vol. 53, no. 8, p. 2417–2421.

[5] NASHAAT, D. M., ELSADEK, H. A., GHALI, H. Single feed compact quad-band PIFA antenna for wireless communication applications. *IEEE Transactions on Antennas and Propagation*. 2005, vol. 53, no. 8, p. 2631–2635.

[6] ZHAN, L., RAHMAT-SAMII, Y. Optimization of PIFA-IFA combination in handset antenna designs. *IEEE Transactions on Antennas and Propagation*. 2005, vol. 53, no. 5, p. 1770–1778.

[7] LATIF, S. I., SHAFAI, L., SHARMA, S. K. Bandwidth enhancement and size reduction of microstrip slot antennas. *IEEE Transactions on Antennas and Propagation*. 2005, vol. 53, no. 3, p. 994 to 1003.

[8] ROW, J. S. Dual-frequency triangular planar inverted-F antenna. *IEEE Transactions on Antennas and Propagation*. 2005, vol. 53, no. 2, p. 874–876.

[9] MOLEIRO, R., NUNES, P. Dual-band microstrip patch antenna elements for GSM. In *Proceedings of the Antennas and Propagation Society International Symposium*. 2000, vol. 3, p. 1596–1599.

[10] POLÍVKA, M., DRAHOVZAL, M., MAZÁNEK, M. Synthesis of dualband broadside radiated microstrip patch antenna operating with TM_10 and TM_21 modes. In *Proceedings of the 2004 IEEE Antennas and Propagation Society International Symposium*. Monterey (CA, USA), 2004, p. 245–248.

[11] POLÍVKA, M. Multiband behavior of the rectangular microstrip patch antenna modified by T notch perturbation elements. In *Proceedings of the 18th International Conference on Applied Electromagnetics in Communications ICECom 2005*. Dubrovnik (Croatia): KOREMA, 2005, p. 185–188.

[12] HAZDRA, P. Numerical analysis of microstrip patch antennas with fractal boundary. In *POSTER 2002 – Book of Extended Abstracts*. Prague : CTU – Faculty of Electrical Engineering, 2002, p. C10.

[13] HAZDRA P., MAZÁNEK, M. Planar patch antennas with fractal boundary. In *Proceedings of ISAP 2004*. Sendai (Japan), 2005, p. 401–404.

[14] http://www.cst.com/ – the home site of Computer Simulation Technology Ltd.

[15] http://www.zeland.com – the home site of Zeland Software Inc.

About Authors...

Aleš ČÁP was born in 1977. He is a master student of electronics and telecommunications at the Brno University of Technology. In 2005, he is going to finish his study by defending diploma thesis *Multi-Band Planar Antennas with Perturbation Elements*.

Zbyněk RAIDA (* 1967 in Opava) received Ing. (M.Sc.) and Dr. (Ph.D.) degrees from Brno University of Technology (BUT), Faculty of Electrical Engineering and Communication (FEEC) in 1991 and 1994, respectively.

Since 1993, he has been with the Dept. of Radio Electronics of FEEC BUT as the assistant professor (1993 to 98), associate professor (1999 to 2003), and professor (since 2004). From 1996 to 1997, he spent 6 months at the Laboratoire de Hyperfrequences, Universite Catholique de Louvain, Belgium as an independent researcher. Since 2002, he occupies the position of the vicedean for research and doctoral study at FEEC.

Prof. Raida has authored or coautored more than 80 papers in scientific journals and conference proceedings. His research has been focused on numerical modeling and optimization of electromagnetic structures, application of neural networks to modeling and design of microwave structures, and on adaptive antennas. In 1999, he received the Young Scientist Award of URSI General Assembly in Toronto, Canada.

Prof. Raida is a member of the IEEE Microwave Theory and Techniques Society. From 2001 to 2003, he chaired the MTT/AP/ED joint section of the Czech-Slovak chapter of IEEE. In 2003, he became the Senior Member of IEEE.

Since 2001, Prof. Raida is editor-in-chief of the Radioengineering journal (publication of Czech and Slovak Technical Universities and URSI committees).

Eduardo de las HERAS PALMERO was born in 1979. He is a student of the University of Cantabria (Spain) of Telecommunication Engineering. In 2005, he is going to finish his studies working in his master's thesis in a project at the Brno University of Technology.

Roberto LAMADRID RUIZ was born in 1979. He is a student of the University of Cantabria of Telecommunication Engineering. He received the B.S. degree in electronic systems and telecommunication in 2004 from the University of Cantabria. His Bachelor's thesis was about the design and measurements of a LMDS system. In 2005, he is going to finish his studies working in his master's thesis in a project at the Brno University of Technology.